scientific reports

Check for updates

OPEN

Impaired regulation of heart rate and sinoatrial node function by the parasympathetic nervous system in type 2 diabetic mice

Yingjie Liu[1,2], Hailey J. Jansen[1,2], Pooja S. Krishnaswamy[3], Oleg Bogachev[3] & Robert A. Rose[1,2]✉

Heart rate (HR) and sinoatrial node (SAN) function are modulated by the autonomic nervous system. HR regulation by the parasympathetic nervous system (PNS) is impaired in diabetes mellitus (DM), which is denoted cardiovascular autonomic neuropathy. Whether blunted PNS effects on HR in type 2 DM are related to impaired responsiveness of the SAN to PNS agonists is unknown. This was investigated in type 2 diabetic db/db mice in vivo and in isolated SAN myocytes. The PNS agonist carbachol (CCh) had a smaller inhibitory effect on HR, while HR recovery time after CCh removal was accelerated in db/db mice. In isolated SAN myocytes CCh reduced spontaneous action potential firing frequency but this effect was reduced in db/db mice due to blunted effects on diastolic depolarization slope and maximum diastolic potential. Impaired effects of CCh occurred due to enhanced desensitization of the acetylcholine-activated K^+ current (I_{KACh}) and faster I_{KACh} deactivation. I_{KACh} alterations were reversed by inhibition of regulator of G-protein signaling 4 (RGS4) and by the phospholipid PIP_3. SAN expression of RGS4 was increased in db/db mice. Impaired PNS regulation of HR in db/db mice occurs due to reduced responsiveness of SAN myocytes to PNS agonists in association with enhanced RGS4 activity.

Heart rate (HR), which is a critical determinant of cardiac performance, is determined by the intrinsic properties of the sinoatrial node (SAN) and is modulated by the autonomic nervous system (ANS)[1,2]. The sympathetic nervous system (SNS) increases HR by enhancing SAN activity while the parasympathetic nervous system (PNS) reduces HR via the actions of acetylcholine on muscarinic receptors (M_2R) in the SAN[2].

In diabetes mellitus (DM), cardiovascular complications are highly prevalent, leading to death and morbidity in DM patients. HR regulation by the ANS is known to be impaired in DM patients, which has been attributed to a condition denoted cardiovascular autonomic neuropathy (CAN)[3,4]. CAN, which can be associated with damage to the nerves that innervate the heart, can affect up to 90% of DM patients and increases mortality by two- to five-fold compared to DM patients without CAN[3,5]. Although nerve damage may be involved in the impairments in HR regulation by the PNS, it is also possible that these impairments may occur due to alterations in PNS signaling within the SAN.

SAN myocytes generate spontaneous action potentials (APs), which set the intrinsic HR, in association with a diastolic depolarization (DD) that occurs between successive APs[2]. The DD is generated by a number of ionic currents including the hyperpolarization-activated current (I_f), which is generated by hyperpolarization-activated cyclic nucleotide gated (HCN) channels, and a rapidly-activating delayed rectifier K^+ currents (I_{Kr}), which is generated by *ether-a-go-go* (ERG) channels[1,6]. The PNS reduces HR via the activation of inhibitory G proteins (G_i) associated with M_2Rs. Key mediators of this reduction in HR are the acetylcholine-activated K^+ current (I_{KACh}; generated by $K_{ir}3.1$ and $K_{ir}3.4$ channels) and I_f[1,7]. Specifically, activation of I_{KACh} by the βγ subunit of the G_i protein results in hyperpolarization of the maximum diastolic potential (MDP) in SAN myocytes while inhibition of I_f

[1]Department of Cardiac Sciences, Libin Cardiovascular Institute, Cumming School of Medicine, University of Calgary, GAC66, Health Research Innovation Centre, 3280 Hospital Drive N.W., Calgary, AB T2N 4Z6, Canada. [2]Department of Physiology and Pharmacology, Libin Cardiovascular Institute, Cumming School of Medicine, University of Calgary, GAC66, Health Research Innovation Centre, 3280 Hospital Drive N.W., Calgary, AB T2N 4Z6, Canada. [3]Department of Physiology and Biophysics, Dalhousie University, Halifax, NS, Canada. ✉email: robert.rose@ucalgary.ca

downstream of $G_{\alpha i}$ and a reduction in cyclic AMP (cAMP) reduces the slope of the DD in SAN myocytes. Both effects contribute importantly to a slowing of spontaneous AP firing in SAN myocytes.

Previous studies have shown that regulation of HR by the PNS is impaired in type 1 DM (T1DM) and that this occurs in association with altered responsiveness to PNS agonists in the SAN[8,9]. Type 2 DM (T2DM) accounts for up to 90% of all DM patients and is also associated with impaired PNS activity[4,10]. Importantly, blunted PNS activity and CAN present earlier in T2DM patients compared to T1DM[4]; however, the basis for this is unknown making studies of dysregulation of HR by the PNS specifically in T2DM essential. Accordingly, the purpose of this study was to investigate the regulation of HR and SAN function by the PNS using db/db mice, a model of obesity and T2DM[11].

Methods

An expanded methods section is available in the Supplementary Information.

Animals. This study used male and female littermate wildtype and db/db (strain: C57BL/gj-*Lepr*^{db}) mice between 16 and 20 weeks of age. The db/db mice contain a mutation in the leptin receptor (*Lepr*) gene leading to hyperphagia[11]. These db/db mice exhibit the expected features of T2DM including obesity and hyperglycemia, as we[12] and others[13,14] have shown. All experimental procedures were approved by the University of Calgary Animal Care and Use Committee or the Dalhousie University Committee for Laboratory Animals and were in accordance with the guidelines of the Canadian Council on Animal Care and the ARRIVE guidelines.

Intracardiac electrophysiology and electrocardiogram recording. HR was measured from lead II surface electrocardiograms (ECGs) and corrected SAN recovery time (cSNRT) was measured using an octapolar electrophysiology catheter in anesthetized mice as described previously[8,15,16] and in the Supplementary Information.

Patch-clamping of isolated sinoatrial node myocytes. Isolated SAN myocytes were used to record spontaneous APs and ionic currents, including I_f and I_{Kr}, using the whole cell patch-clamp technique in current clamp or voltage clamp mode, respectively. The protocols and solutions for these experiments are described in the Supplementary Information.

Quantitative polymerase chain reaction and Western blotting. Quantitative gene expression was measured in isolated SAN tissue as previously described[16,17]. Western blotting was performed using isolated SAN tissue as described previously[16]. The experimental protocols for these techniques are described in the Supplementary Information.

Statistical analysis. All data are presented as means ± SEM. Data were analyzed using two-way ANOVA with the Holm–Sidak posthoc test or Student's *t*-test as indicated in each figure legend. $P < 0.05$ was considered significant.

Results

Effects of carbachol on heart rate and sinoatrial node function in db/db diabetic mice. ECG recordings in anesthetized mice (Fig. 1A) demonstrate that HR was lower in db/db mice at baseline and that the ability of the PNS agonist carbachol (CCh; 0.1 mg/kg intraperitoneal injection) to reduce HR was reduced compared to wildtype mice (Fig. 1B,C). The kinetics of the effects of CCh on HR, and the return of HR to baseline after application of the muscarinic (M_2) receptor blocker atropine (10 mg/kg, intraperitoneal injection), are presented in Fig. 1D–F. These data further demonstrate that the ability of CCh to reduce HR is impaired in db/db mice and that the return to baseline HR after application of atropine occurs faster in db/db mice (Fig. 1D–F). Impaired HR regulation by CCh in db/db mice was also studied by directly assessing SAN function, as determined by corrected SAN recovery time (cSNRT), in vivo (Fig. 2A). cSNRT was longer at baseline in db/db mice. Application of CCh (0.1 mg/kg) prolonged cSNRT; however, this response was reduced in db/db mice (Fig. 2B,C). These data indicate that the effects of CCh on HR are reduced in db/db mice and that this is associated with impaired responsiveness of the SAN to PNS agonists.

Effects of CCh on SAN myocyte electrophysiology in db/db mice. To determine the basis for the impaired effects of CCh on HR, spontaneous APs were recorded in isolated SAN myocytes from db/db and wildtype mice (Fig. 3A). SAN AP frequency was lower at baseline in db/db mice. CCh (50 nM) reduced SAN AP frequency, but this effect was smaller in db/db SAN myocytes compared to wildtype (Fig. 3B). Consistent with this, CCh elicited a smaller reduction in DD slope (Fig. 3C) and failed to produce a statistically significant hyperpolarization of the MDP (Fig. 3D) in db/db SAN myocytes. These responses were similar in SAN myocytes isolated from male and female db/db and wildtype mice (Supplementary Fig. S1).

The absence of a normal hyperpolarization of the MDP suggests a key role for I_{KACh} in the blunted response to CCh in db/db mice. Thus, I_{KACh} was investigated next. Figure 4A illustrates representative recordings at baseline, at the peak of the CCh (10 µM) response and 2 min after the peak CCh response when I_{KACh} has undergone desensitization. Peak I_{KACh} (i.e. peak of the CCh activated I_K) was not different between wildtype and db/db SAN myocytes (Fig. 4B). In contrast, plotting the time course of the effects of CCh on I_{KACh} (measured at − 100 mV; Fig. 4C) revealed that I_{KACh} desensitization (i.e. the reduction in I_{KACh} amplitude that occurs in the presence of CCh following peak response) was increased (Fig. 4D) and I_{KACh} recovery time (i.e. deactivation) during CCh

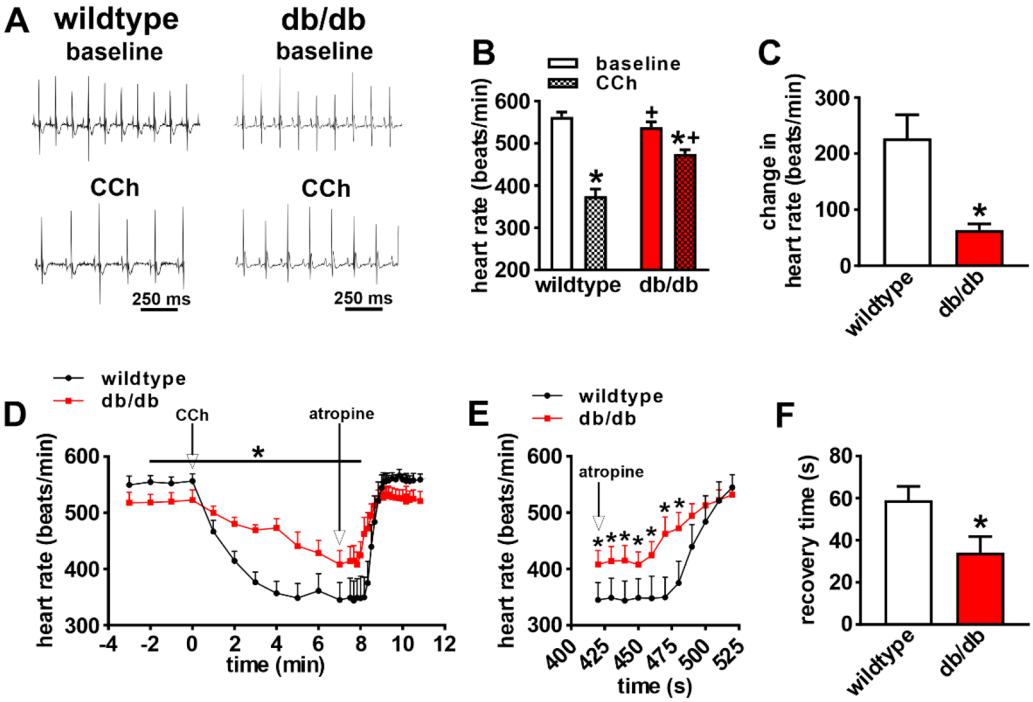

Figure 1. Effects of carbachol on heart rate in db/db mice in vivo. (**A**) Representative surface ECGs in baseline conditions and after application of CCh (0.1 mg/kg) in anesthetized wildtype and db/db mice. (**B**) Summary of heart rate at baseline and after CCh in wildtype ($n=9$) and db/db ($n=13$) mice. $^{*}P<0.05$ vs baseline; $^{+}P<0.05$ vs. wildtype by two-way ANOVA with Holm–Sidak posthoc test. (**C**) Change in heart rate after CCh application in wildtype and db/db mice. $^{*}P<0.05$ vs. wildtype by Student's t-test. (**D**) Time course of changes in heart rate after application of CCh and atropine (10 mg/kg) in wildtype ($n=5$) and db/db ($n=6$) mice. (**E**) Magnified region of data from panel D illustrating the changes in heart rate upon application of atropine in wildtype and db/db mice. For panels (**D**) and (**E**) $^{*}P<0.05$ vs. wildtype by two-way repeated measures ANOVA with Holm–Sidak posthoc test. (**F**) Recovery time for heart rate after application of atropine. $^{*}P<0.05$ vs. wildtype by Student's *t*-test.

washout was faster (Fig. 4E) in db/db SAN myocytes compared to wildtype. There were no differences in expression of *Chrm2* mRNA or M_2R protein in the SAN in db/db mice (Supplementary Fig. S2). While the mRNA expression of *Kcnj3* was reduced, there were no differences in the expression of *Kcnj5*, or the corresponding proteins, $K_{ir}3.1$ and $K_{ir}3.4$, in the SAN in db/db mice (Supplementary Fig. S3). These data demonstrate that I_{KACh} is impaired in db/db SAN myocytes due to enhanced desensitization and faster deactivation kinetics.

CCh can also reduce SAN AP firing by inhibiting I_f. Accordingly, the effects of CCh on I_f in db/db SAN myocytes were investigated. CCh (10 µm) reduced I_f density in wildtype and db/db SAN myocytes (Fig. 5A–C). Comparison of these effects illustrates that I_f tended to be smaller at baseline in db/db SAN myocytes and that I_f was reduced similarly in both genotypes following application of CCh (Fig. 5D). CCh reduced I_f in association with a hyperpolarizing shift in the I_f activation curve (Fig. 5E,F). There were no differences in the voltage dependence of activation ($V_{1/2(act)}$) at baseline or after CCh in wildtype and db/db SAN myocytes (Fig. 5G) indicating that the effects of CCh on I_f were similar between both groups of mice. There were also no differences in the mRNA expression or protein levels of HCN1, HCN2 or HNC4 in the SAN of db/db mice (Supplementary Fig. S4). These data demonstrate that impaired SAN responsiveness to PNS agonists is not related to altered effects of CCh on I_f.

Since baseline spontaneous AP firing and DD slope were reduced in db/db SAN myocytes, and this wasn't accounted for by differences in baseline I_f, other mechanisms were explored. Repolarizing I_K was reduced in db/db SAN myocytes (Supplementary Fig. S5). Furthermore, voltage clamp protocols designed to detect I_{Kr} tail currents revealed that I_{Kr} is reduced in db/db SAN myocytes (Supplementary Fig. S5). This reduction occurred without changes in $V_{1/2(act)}$ or slope factor (k) for I_{Kr} tail currents (Supplementary Fig. S5). I_{Kr} has been shown to be a critical determinant of SAN spontaneous AP firing and DD slope[18] suggesting that the reduction in I_{Kr} could account for baseline differences in spontaneous AP firing in db/db mice.

Altered RGS4 and PIP_3 signaling underlie impaired I_{KACh} in db/db SAN myocytes. Previous studies have shown that I_{KACh} desensitization and deactivation kinetics are critically affected by regulator of G protein signaling 4 (RGS4) in the SAN[19]. Furthermore, RGS4 is inhibited by phosphatidylinositol (3,4,5) P_3 (PIP_3)[20] which is activated by insulin-mediated PI3K signaling[21,22]. Therefore, impaired insulin and PI3K signaling in T2DM could result in enhanced RGS4 activity due to a loss of PIP_3-mediated inhibition of RGS4. To test this hypothesis, wildtype and db/db SAN myocytes were dialyzed with the RGS4 inhibitor CCG-4986 (10 µM)

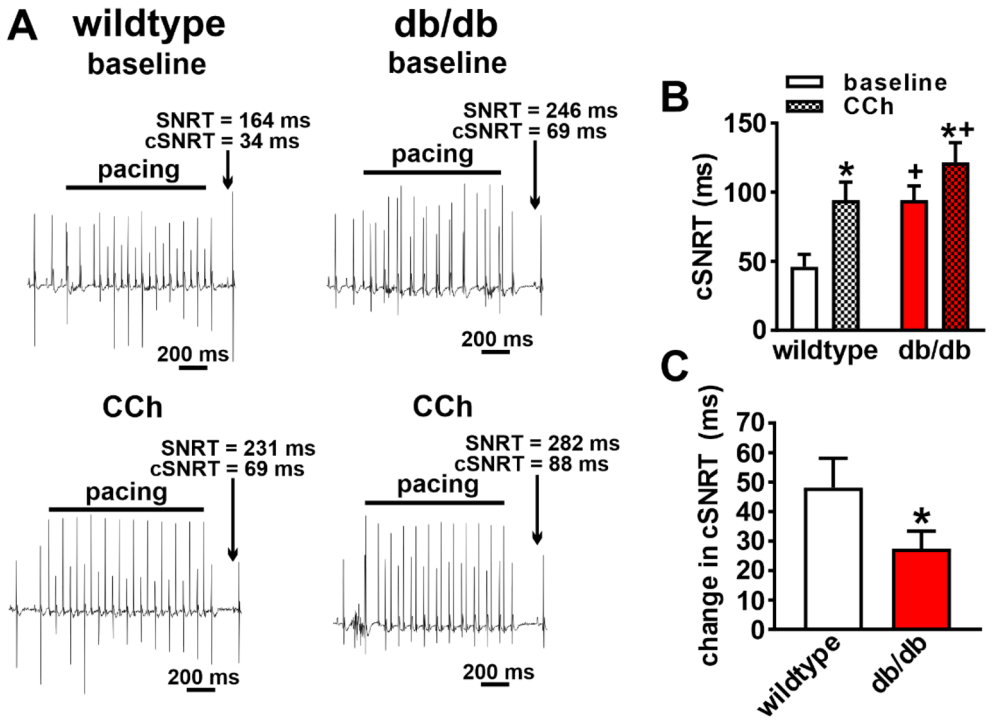

Figure 2. Effects of carbachol on sinoatrial node recovery time in db/db mice in vivo. (**A**) Representative recordings illustrating assessment of corrected sinoatrial node recovery time (cSNRT) at baseline and after CCh (0.1 mg/kg) in wildtype and db/db mice. (**B**) Summary of cSNRT at baseline and after CCh in wildtype ($n=7$) and db/db ($n=11$) mice. $^{*}P<0.05$ vs baseline; $^{+}P<0.05$ vs. wildtype by two-way ANOVA with Holm–Sidak posthoc test. (**C**) Change in cSNRT after CCh application in wildtype and db/db mice. $^{*}P<0.05$ vs. wildtype by Student's *t*-test.

for 10 min prior to studying the effects of CCh (10 μM) on I_{KACh} (Fig. 6A). Time course plots demonstrate that I_{KACh} desensitization and deactivation kinetics were normalized in db/db SAN myocytes after CCG-4986 application (Fig. 6B). Summary data demonstrate that there were no differences in peak I_{KACh} density (Fig. 6C), I_{KACh} desensitization (Fig. 6D) or I_{KACh} recovery time (Fig. 6E) between wildtype and db/db SAN myocytes following inhibition of RGS4 with CCG-4986. RGS4 mRNA expression and protein levels were increased in the SAN in db/db mice (Fig. 7).

Next, wildtype and db/db SAN myocytes were dialyzed with PIP_3 (1 μM) for 10 min prior to application of CCh (10 μM) to investigate I_{KACh} properties (Fig. 8A). Similar to RGS4 inhibition, time course plots demonstrate that I_{KACh} desensitization and deactivation were normalized in db/db SAN myocytes treated with PIP_3 (Fig. 8B). On average, peak I_{KACh} density (Fig. 8C), I_{KACh} desensitization (Fig. 8D) and I_{KACh} recovery time (Fig. 8E) were not different between wildtype and db/db SAN myocytes when treated with PIP_3.

In control experiments, wildtype and db/db SAN myocytes were dialyzed with phosphatidylinositol 4,5-bisphosphate (PIP_2), a phospholipid that does not directly inhibit RGS4 or mediate the actions of insulin-dependent PI3K signaling. PIP_2 (1 μM) was dialyzed into SAN myocytes for 10 min prior to application of CCh to investigate I_{KACh} (Fig. 8F). Time course plots demonstrate that in the presence of PIP_2, I_{KACh} desensitization remained enhanced and I_{KACh} deactivation was faster in db/db SAN myocytes (Fig. 8G). Summary data show that in the presence of PIP_2, peak I_{KACh} density was not different (Fig. 8H), but that I_{KACh} desensitization tended to be increased (Fig. 8I) and recovery time was faster (Fig. 8J) in db/db SAN myocytes compared to wildtype.

Discussion

The present study demonstrates that db/db mice display impaired responsiveness to the PNS agonist CCh in the SAN leading to impaired HR regulation, indicating that this mouse model of T2DM reproduces the phenotype of impaired ANS regulation of the heart seen in T2DM patients. Furthermore, the present study provides novel insight into the cellular and molecular mechanisms leading to blunted PNS regulation of HR in T2DM. In isolated SAN myocytes, CCh displayed a reduced ability to slow spontaneous AP firing in association with a smaller reduction in DD slope and less hyperpolarization of the MDP in db/db mice. In fact, CCh failed to produce a statistically significant hyperpolarization in db/db SAN myocytes. These responses were similar between male and female db/db mice.

Consistent with these effects, I_{KACh} was centrally involved in the impaired effects of CCh on AP firing in SAN myocytes. Analysis of I_{KACh} properties revealed that the peak I_{KACh} density was not altered in db/db SAN myocytes. Similarly, there were no major changes in gene or protein expression of M_2R or $K_{ir}3$ channels in the SAN in db/db mice. Rather, the major alterations in I_{KACh} in db/db SAN myocytes were an increase in desensitization

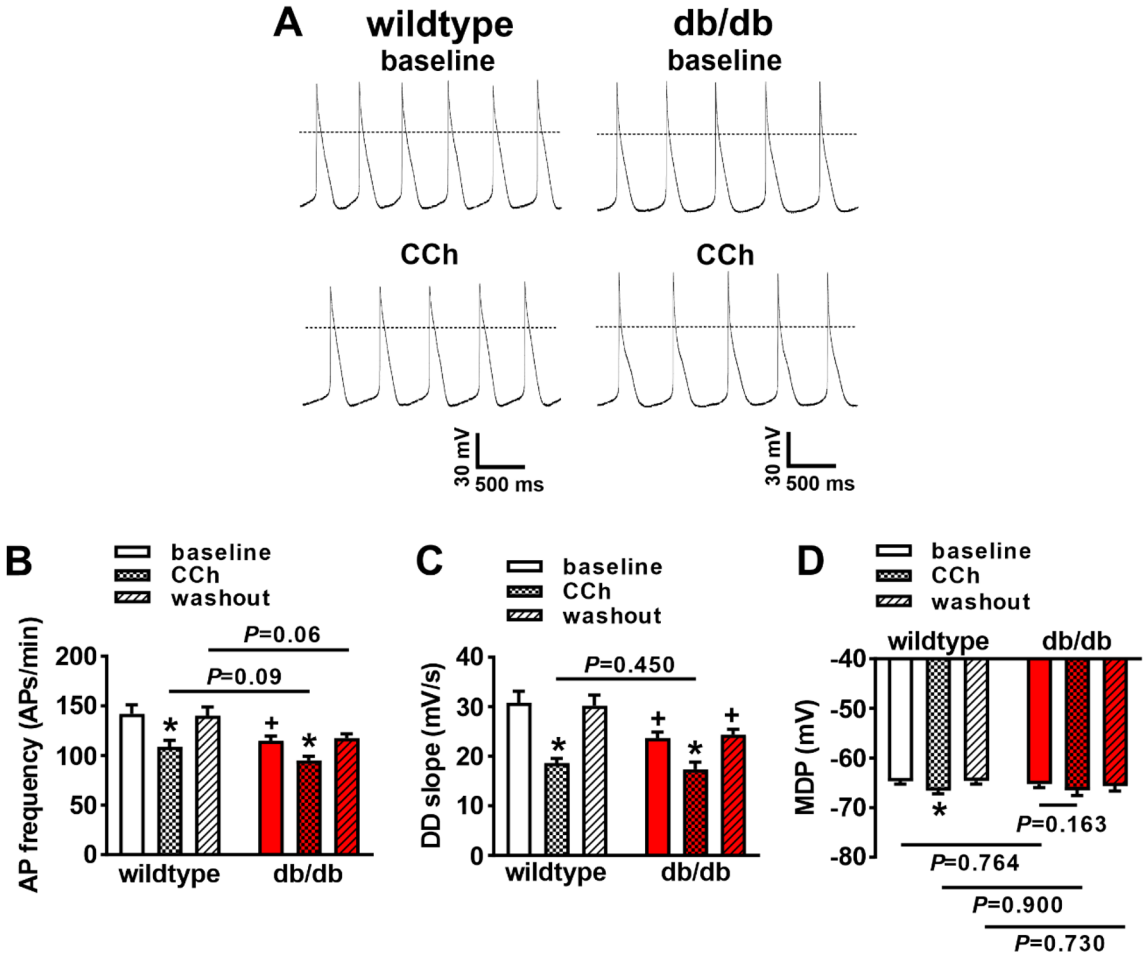

Figure 3. Effects of carbachol on spontaneous action potential firing in isolated sinoatrial node myocytes from db/db mice. (**A**) Representative spontaneous APs at baseline and after CCh (50 nM) in wildtype and db/db SAN myocytes. Dashed lines are at 0 mV. (**B**) Summary of spontaneous AP frequency at baseline and after CCh in wildtype and db/db SAN myocytes. (**C**) Summary of DD slope at baseline and after CCh in wildtype and db/db SAN myocytes. (**D**) Summary of maximum diastolic potential (MDP) at baseline and after CCh in wildtype and db/db SAN myocytes. For panels (**B**–**D**) $n = 14$ wildtype and 13 db/db SAN myocytes; $^{*}P < 0.05$ vs baseline; $^{+}P < 0.05$ vs wildtype by two-way ANOVA with Holm–Sidak posthoc test.

and faster deactivation kinetics. These findings are consistent with our studies in vivo, which demonstrated that the effects of CCh were reduced in db/db mice (likely in association with enhanced desensitization of I_{KACh}) and that reversal of the effects of CCh upon application of atropine was much more rapid in db/db mice (likely in association with faster I_{KACh} deactivation). Both of these effects resulted in impaired PNS effects on HR (and SAN function) over the full time-course of CCh application and removal. Our findings are also consistent with previous studies demonstrating that I_{KACh} plays a critical role in mediating SAN and HR responses to CCh[23,24].

I_{KACh} is well known to undergo a process of desensitization whereby current amplitude decreases in the presence of M_2R agonists such as CCh[25–27]. I_{KACh} desensitization, as well as deactivation are critically affected by regulator of G protein signaling (RGS) proteins, including RGS4, which is highly expressed in the SAN[19,28]. Genetic ablation of RGS4 leads to enhanced PNS signaling due to reductions in I_{KACh} desensitization and slower I_{KACh} deactivation[19]. Thus, increased I_{KACh} desensitization and faster deactivation in db/db SAN myocytes (i.e. the opposite of RGS4 ablation) suggested enhanced RGS4 activity in db/db mice. This was confirmed using CCG-4986, which is a selective RGS4 inhibitor at the doses used in this study[29,30]. These findings are consistent with previous studies demonstrating an essential role for RGS proteins in regulated PNS signaling in the heart via effects on I_{KACh}[19,28,31–33].

RGS4 is importantly regulated by PIP_3, which exerts an inhibitory effect on RGS4 activity[20,34,35]. In the normal heart, PIP_3 is generated from PIP_2 through the actions of PI3Kα (p100α isoform)[21]. In T2DM, impaired insulin signaling results in reduced PI3K activity, which would result in less PIP_3 generation[22,36]. This loss of PIP_3 would lead to less inhibition of RGS4 and could underlie increased RGS4 activity in the SAN of db/db mice. In support of this, bypassing insulin signaling and directly dialyzing db/db SAN myocytes with PIP_3 normalized I_{KACh} desensitization and deactivation. Thus, the studies conducted here demonstrate that the kinetic properties of I_{KACh} are altered in T2DM due to the loss of PIP_3 mediated inhibition of RGS4 and that this is a major determinant of impaired PNS signaling to the SAN and HR regulation in T2DM.

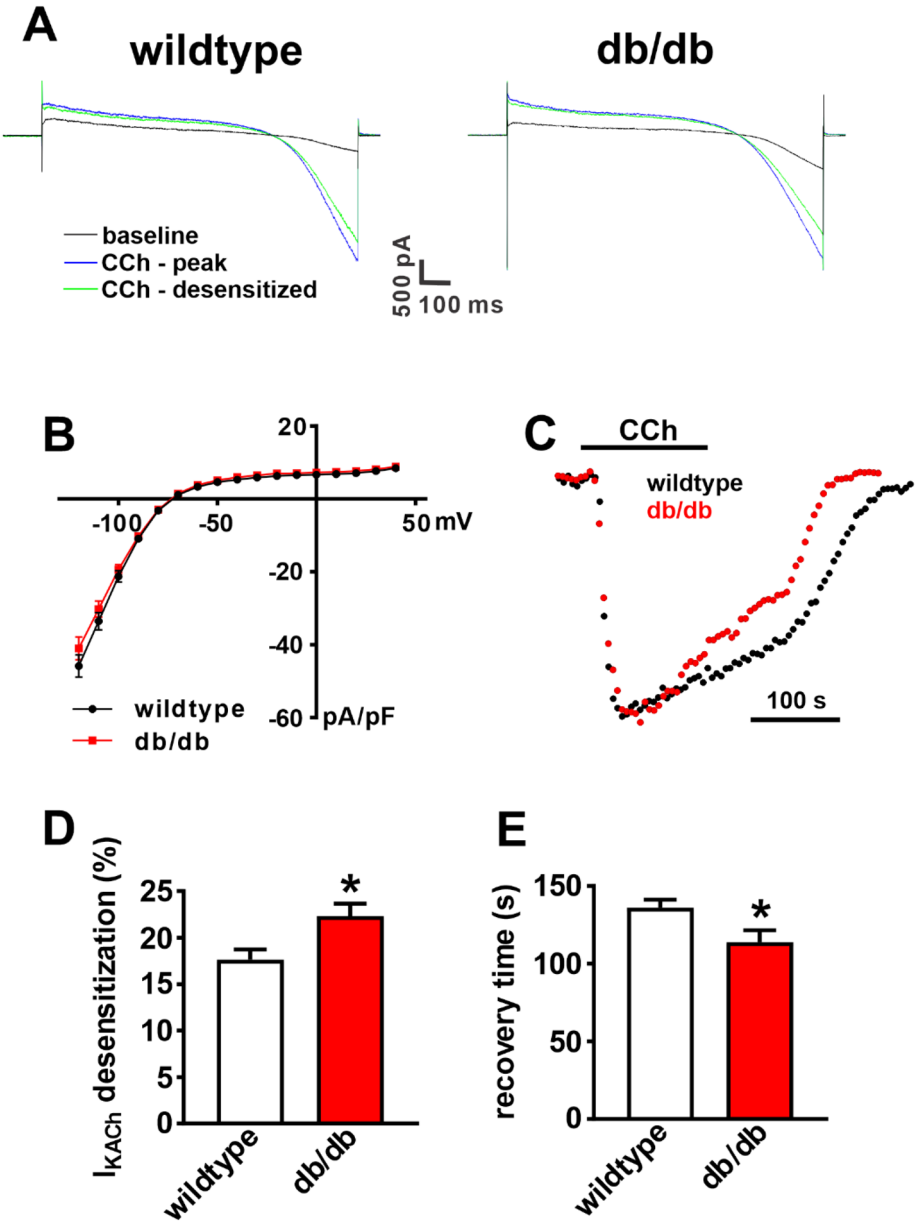

Figure 4. I_{KACh} properties in isolated SAN myocytes from db/db mice. (**A**) Representative I_K recordings during a voltage ramp from + 50 mV to − 120 mV (holding potential = − 80 mV) at baseline, at the peak of the CCh (10 μM) response and 2 min after the peak CCh response in wildtype and db/db SAN myocytes. (**B**) Peak I_{KACh} I–V relationship in wildtype ($n = 28$) and db/db ($n = 25$) SAN myocytes. $P = 0.998$ for wildtype vs. db/db by two-way repeated measures ANOVA with Holm–Sidak posthoc test. (**C**) Time course of CCh stimulated I_{KACh}, measured at − 100 mV, in wildtype and db/db SAN myocytes. (**D**) Summary of I_{KACh} desensitization in wildtype and db/db SAN myocytes. (**E**) Summary of I_{KACh} recovery time during CCh washout in wildtype and db/db SAN myocytes. For panels (**D**,**E**) $^*P < 0.05$ vs. wildtype by Student's *t*-test.

CCh can also reduce spontaneous AP firing by inhibiting I_f, which was also investigated in the present study. As expected, CCh reduced I_f density in association with a hyperpolarizing shift in the $V_{1/2(act)}$; however, this effect was similar in wildtype and db/db SAN myocytes. This indicates that HCN channel function was not altered by a change in RGS4 activity in T2DM. CCh can also modulate SAN activity via other mechanisms such as L-type Ca^{2+} currents and SR Ca^{2+} handling[1,6]. These targets were not investigated in this study; therefore, whether the effects of CCh on these targets are altered in db/db mice and whether these targets are regulated by RGS4 is presently unknown. These could be areas for future study. Nevertheless, the absence of altered CCh effects on I_f (which is also an important mediator of PNS signaling in the SAN) in db/db mice suggests that the effects of RGS4 are selective for $K_{ir}3$ channels. In addition to RGS4, RGS6 has also been shown to regulate I_{KACh} kinetics in the SAN[33,37]. Whether RGS6 is regulated by PIP_3 in similar ways to RGS4 and whether RGS6 contributes to impaired PNS signaling in DM is not currently known.

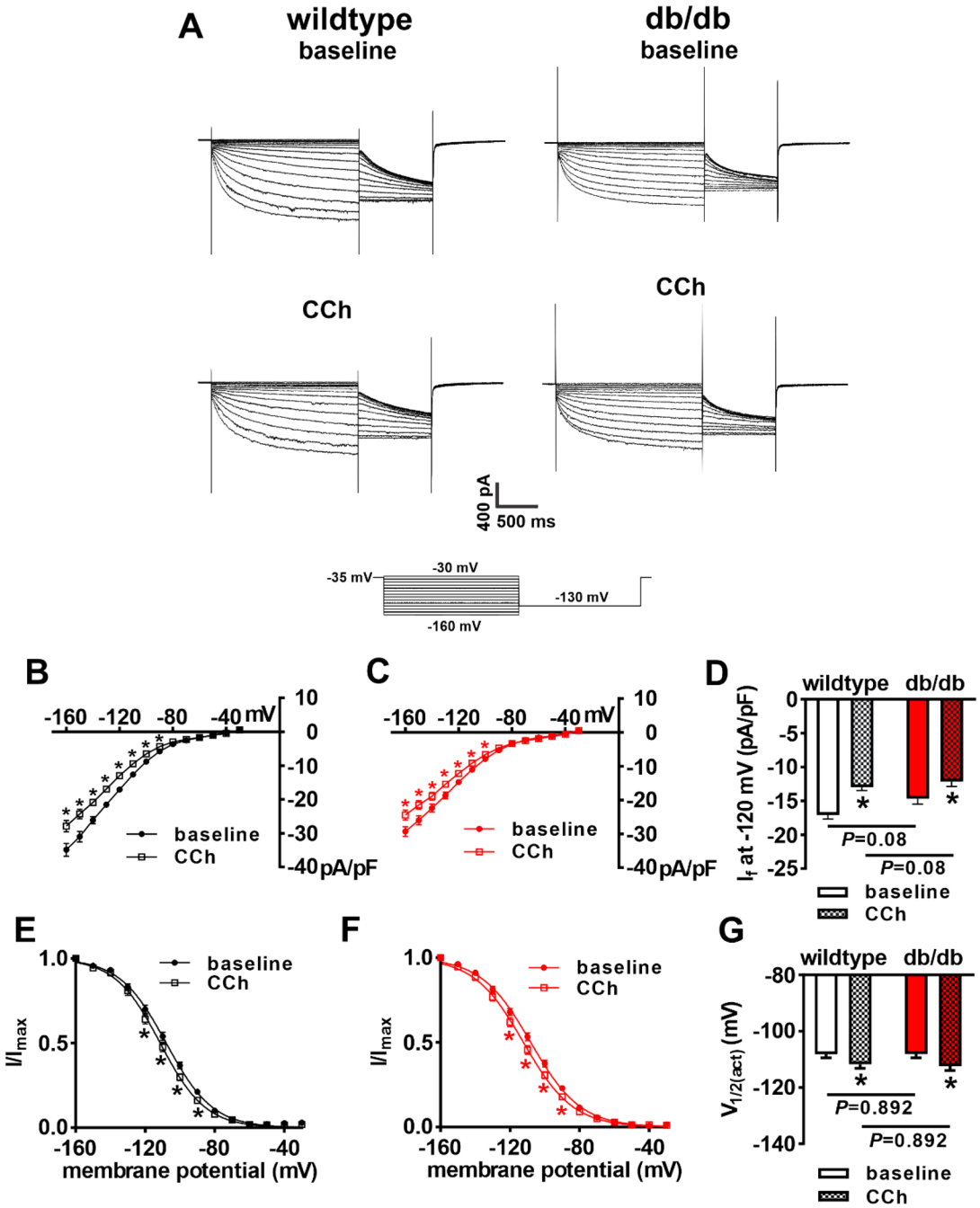

Figure 5. Effects of carbachol on the hyperpolarization-activated current (I_f) in db/db SAN myocytes. (**A**) Representative I_f recordings at baseline and after CCh (10 μM) application in wildtype and db/db SAN myocytes. Voltage clamp protocol shown at bottom of recordings. (**B**) I_f IV curves at baseline and after CCh application in wildtype SAN myocytes ($n = 15$). (**C**) I_f IV curves at baseline and after CCh application in db/db SAN myocytes ($n = 16$). For panels (**B**) and (**C**) $^*P < 0.05$ vs. baseline by two-way repeated measures ANOVA with Holm–Sidak posthoc test. (**D**) I_f density at − 120 mV at baseline and after CCh application in wildtype and db/db SAN myocytes. $^*P < 0.05$ vs baseline by two-way ANOVA with Holm–Sidak posthoc test. (**E**) I_f steady-state activation curves at baseline and after CCh application in wildtype SAN myocytes ($n = 15$). (**F**) I_f steady-state activation curves at baseline and after CCh application in db/db SAN myocytes ($n = 16$). (**G**) I_f $V_{1/2(act)}$ at baseline and after CCh application in wildtype and db/db SAN myocytes. $^*P < 0.05$ vs. baseline by two-way ANOVA with Holm–Sidak posthoc test. Refer to Supplementary Table 1 for additional analysis of I_f steady-state activation.

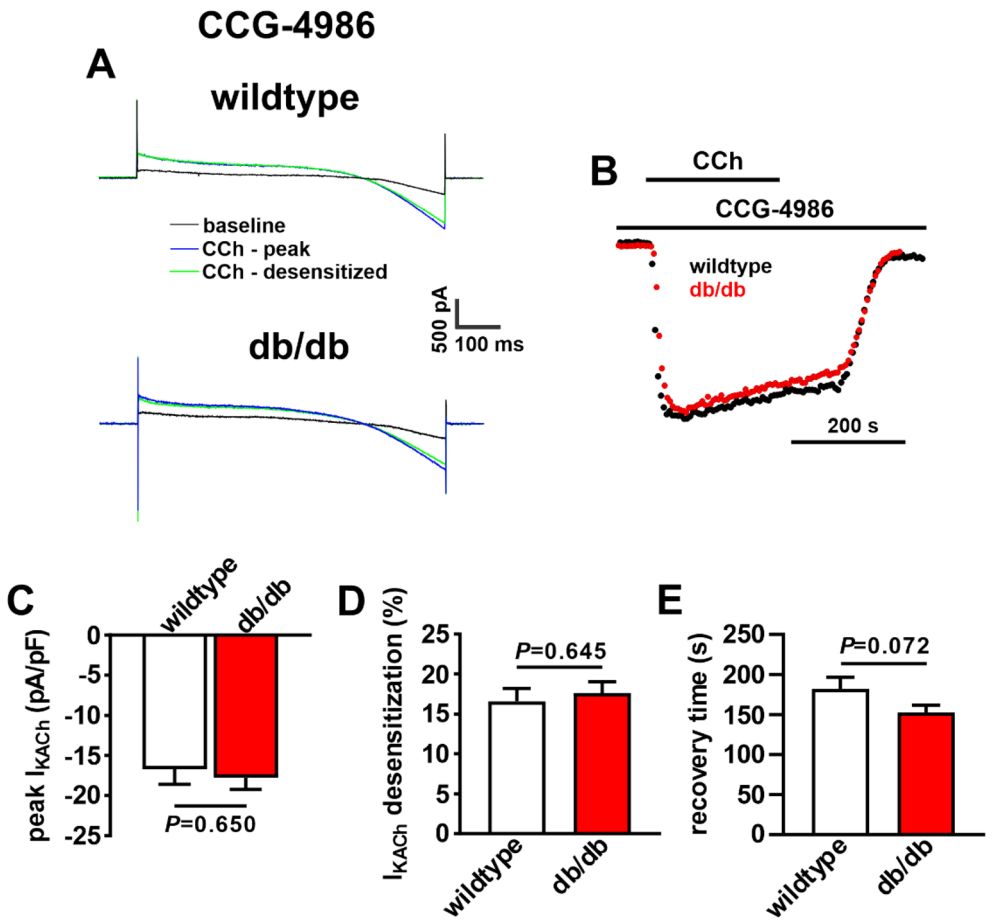

Figure 6. Effects of RGS4 inhibition on I_{KACh} kinetics in db/db SAN myocytes. (**A**) Representative I_K recordings illustrating peak and desensitized responses to CCh (10 μM) in wildtype and db/db SAN myocytes pre-treated with the RGS4 inhibitor CCG-4986 (10 μM). (**B**) Time course of CCh stimulated I_{KACh}, measured at − 100 mV, in wildtype and db/db SAN myocytes in the presence of CCG-4986. (**C**) Summary of peak I_{KACh} at − 100 mV in wildtype and db/db SAN myocytes in the presence of CCG-4986. (**D**) Summary of I_{KACh} desensitization in wildtype and db/db SAN myocytes in the presence of CCG-4986. (**E**) Summary of I_{KACh} recovery time during CCh washout in wildtype and db/db SAN myocytes in the presence of CCG-4986. For panels (**C**–**E**) $n = 16$ wildtype and 18 db/db SAN myocytes; data analyzed by Student's *t*-test.

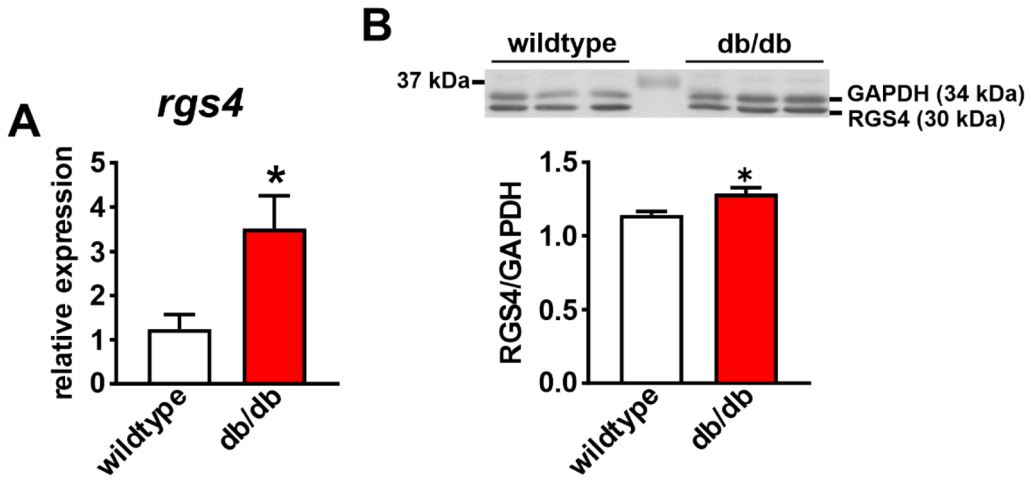

Figure 7. RGS4 gene and protein expression in the SAN in db/db mice. (**A**) mRNA expression of *rgs4* in wildtype ($n = 5$) and db/db ($n = 5$) SAN. *$P < 0.05$ vs wildtype by Student's *t*-test. (**B**) Representative Western blot and summary protein expression for RGS4 in the SAN of wildtype ($n = 6$) and db/db ($n = 6$) mice. *$P < 0.05$ vs. wildtype by Student's *t*-test. Uncropped Western blot provided in Supplementary Fig. S6.

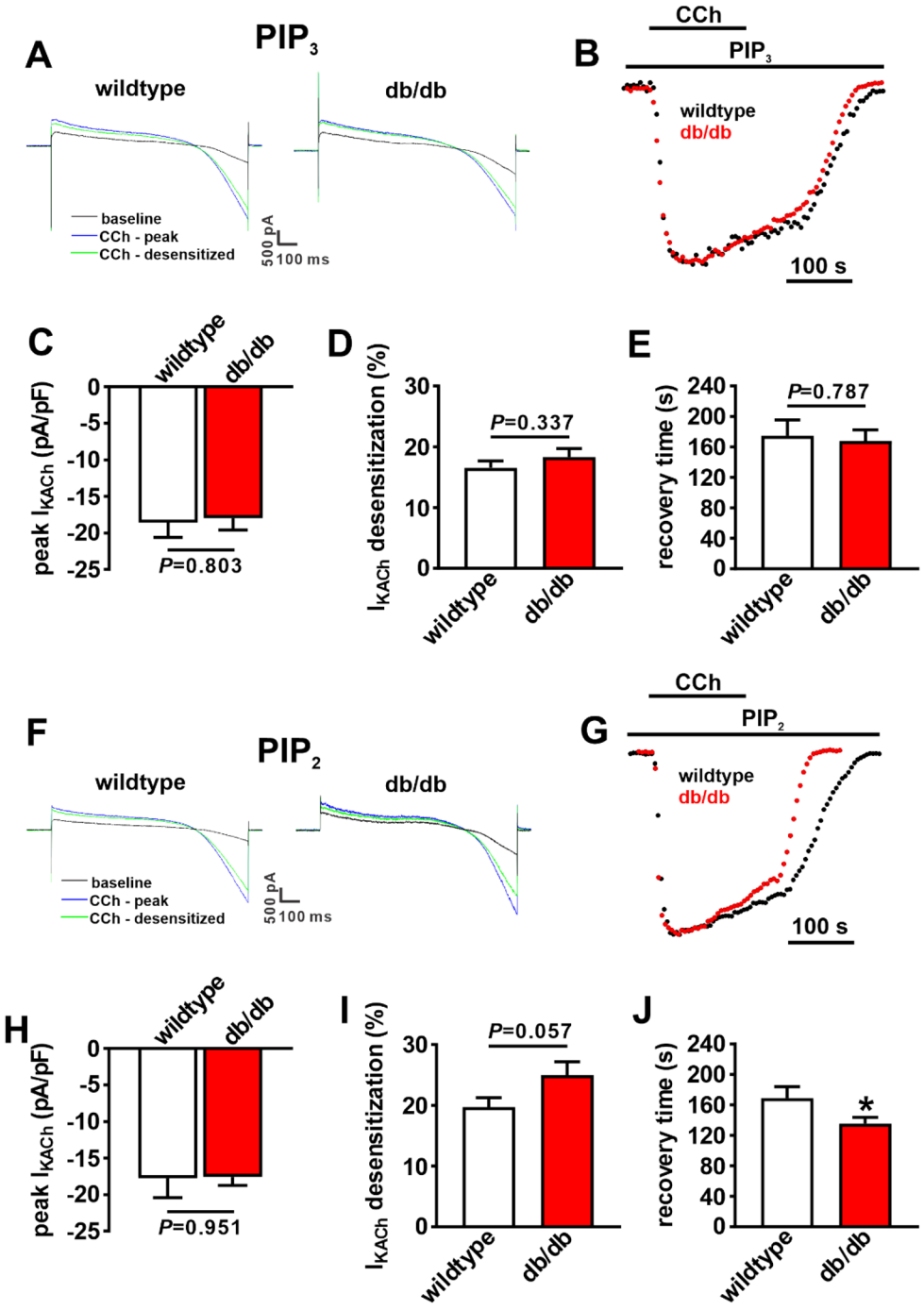

Figure 8. Effects of PIP_3 on I_{KACh} kinetics in db/db SAN myocytes. (**A**) Representative I_K recordings illustrating peak and desensitized responses to CCh in wildtype and db/db SAN myocytes dialyzed with PIP_3 (1 μM). (**B**) Time course of CCh stimulated I_{KACh}, measured at − 100 mV, in wildtype and SAN myocytes dialyzed with PIP_3. (**C**-**E**) Summary of peak I_{KACh} at − 100 mV (**C**), I_{KACh} desensitization (**D**) and I_{KACh} recovery time during CCh washoff (**E**) in wildtype ($n = 16$) and db/db ($n = 19$) SAN myocytes dialyzed with PIP_3. Data in panels (**C**–**E**) analyzed by Student's *t*-test. (**F**) Representative I_K recordings illustrating peak and desensitized responses to CCh in wildtype and db/db SAN myocytes dialyzed with PIP_2 (1 μM). (**G**) Time course of CCh stimulated I_{KACh}, measured at − 100 mV, in wildtype and SAN myocytes dialyzed with PIP_2. (**H**–**J**) Summary of peak I_{KACh} at − 100 mV (**H**), I_{KACh} desensitization (**I**) and I_{KACh} recovery time during CCh washoff (**J**) in wildtype ($n = 18$) and db/db ($n = 19$) SAN myocytes dialyzed with PIP_2. For panels (**H**–**J**) $^*P < 0.05$ by Student's *t*-test.

PNS signaling in the SAN has also been previously investigated in T1DM using Akita mice[8]. The present study demonstrates that while there are similarities in how PNS signaling is altered in Akita and db/db mice, there are also important differences. Similar to the present study in db/db mice, HR regulation by CCh was impaired in Akita mice in association with impaired responsiveness of SAN myocytes to CCh. I_{KACh} desensitization and deactivation also showed similar changes in Akita SAN myocytes to those identified here in db/db mice and these changes were reversible by RGS4 inhibition or application PIP_3 in both models of DM. Conversely, Akita mice showed no differences in expression of RGS4 in the SAN[8], whereas RGS4 gene and protein expression were increased in the SAN in db/db mice. This indicates that RGS4 plays a central role in impaired PNS signaling in the SAN in T1DM and T2DM, but that there are some differences in how RGS4 is altered in the two forms of DM. The increase in RGS4 expression, in combination with increased RGS4 activity due to loss of PIP_3 signaling, demonstrates that alterations in RGS4 are more complex and multifaceted in db/db mice compared to Akita mice. This could explain, at least in part, the finding that CAN often develops earlier in T2DM compared to T1DM patients[4]. Collectively, these data demonstrate that RGS4 signaling is particularly important in the SAN in type 2 diabetic db/db mice due to multiple alterations including increases in its gene and protein expression as well as its functional regulation by PI3K-PIP_3 signaling.

The present study also shows that baseline HR and spontaneous AP firing in SAN myocytes are reduced in db/db mice. This is consistent with previous studies showing lower HR and impaired SAN function in animal models of T1DM and T2DM[12,38–42]. In the present study, baseline I_f density tended to be lower in db/db SAN myocytes; however, there were no differences in baseline $V_{1/2(act)}$ or in the gene and protein expression of HCN1, HCN2 or HCN4 in db/db mice suggesting I_f does not play a major role in baseline HR differences. I_{Kr} plays an integral role in the SAN where it controls AP repolarization, contributes to the DD slope and helps determine AP firing frequency[18]. We measured I_{Kr} from tail currents, which showed $V_{1/2(act)}$ values very similar to those reported in previous studies for this current[18], and found that I_{Kr} is reduced in db/db SAN myocytes, suggesting that this could contribute to baseline differences in HR and SAN activity in db/db mice. Additional studies will be required to investigate the roles of I_f, I_{Kr} and other ionic mechanisms not assessed in this study in baseline differences in SAN AP firing in db/db mice. Reduced basal HR in vivo in the presence of impaired PNS signaling suggests additional alterations in db/db mice. Baseline HR is determined by intrinsic SAN function, the balance between sympathetic and parasympathetic nervous system regulation of the SAN and other factors such as circulating factors that affect the SAN. Our study suggests that even though PNS signaling is impaired, baseline HR is reduced in part due to impaired intrinsic SAN function. Furthermore, sympathetic nervous system activity was not investigated in this study, but may also be altered in db/db mice. As such, future studies investigating sympathetic regulation of HR and baseline HR differences in db/db mice are warranted.

In summary, the present study provides new insight into the basis for impaired PNS regulation of HR in T2DM. The effects of CCh on HR were reduced in association with impaired responsiveness of SAN myocytes to CCh. I_{KACh}, which is a key mediator of the effects of PNS activation in the SAN, displayed enhanced desensitization and faster deactivation kinetics in db/db SAN myocytes resulting in blunted effects of CCh on HR throughout the duration of CCh exposure and removal. These I_{KACh} alterations occurred due to enhanced RGS4 activity and the loss of PIP_3 signaling in db/db SAN myocytes. These findings, which identify potential new targets for intervention in diabetic patients, should be taken into consideration when interpreting CAN and blunted ANS signaling to the heart in T2DM.

Data availability

Any data or experimental reagents are available from the corresponding author upon reasonable request.

Received: 12 February 2021; Accepted: 31 May 2021
Published online: 14 June 2021

References

1. Mangoni, M. E. & Nargeot, J. Genesis and regulation of the heart automaticity. *Physiol. Rev.* **88**, 919–982 (2008).
2. MacDonald, E. A., Rose, R. A. & Quinn, T. A. Neurohumoral control of sinoatrial node activity and heart rate: Insight from experimental models and findings from humans. *Front. Physiol.* **11**, 170 (2020).
3. Vinik, A. I. & Ziegler, D. Diabetic cardiovascular autonomic neuropathy. *Circulation* **115**, 387–397 (2007).
4. Bakkar, N. Z. *et al.* Cardiac autonomic neuropathy: A progressive consequence of chronic low-grade inflammation in type 2 diabetes and related metabolic disorders. *Int. J. Mol. Sci.* **21**, 9005 (2020).
5. Maser, R. E., Mitchell, B. D., Vinik, A. I. & Freeman, R. The association between cardiovascular autonomic neuropathy and mortality in individuals with diabetes: A meta-analysis. *Diabetes Care* **26**, 1895–1901 (2003).
6. Lakatta, E. G., Maltsev, V. A. & Vinogradova, T. M. A coupled SYSTEM of intracellular Ca2+ clocks and surface membrane voltage clocks controls the timekeeping mechanism of the heart's pacemaker. *Circ. Res.* **106**, 659–673 (2010).
7. DiFrancesco, D. Pacemaker mechanisms in cardiac tissue. *Annu. Rev. Physiol.* **55**, 455–472 (1993).
8. Krishnaswamy, P. S. *et al.* Altered parasympathetic nervous system regulation of the sinoatrial node in Akita diabetic mice. *J. Mol. Cell. Cardiol.* **82**, 125–135 (2015).
9. Park, H. J. *et al.* Role of SREBP-1 in the development of parasympathetic dysfunction in the hearts of type 1 diabetic Akita mice. *Circ. Res.* **105**, 287–294 (2009).
10. Kahn, S. E., Cooper, M. E. & Del Prato, S. Pathophysiology and treatment of type 2 diabetes: Perspectives on the past, present, and future. *Lancet* **383**, 1068–1083 (2014).
11. Hsueh, W. *et al.* Recipes for creating animal models of diabetic cardiovascular disease. *Circ. Res.* **100**, 1415–1427 (2007).
12. Bohne, L. J. *et al.* Electrical and structural remodeling contribute to atrial fibrillation in type 2 diabetic db/db mice. *Heart Rhythm* **18**, 118–129 (2021).

13. Carley, A. N. *et al.* Treatment of type 2 diabetic db/db mice with a novel PPARgamma agonist improves cardiac metabolism but not contractile function. *Am. J. Physiol. Endocrinol. Metab.* **286**, E449-455 (2004).
14. Hafstad, A. D., Solevag, G. H., Severson, D. L., Larsen, T. S. & Aasum, E. Perfused hearts from Type 2 diabetic (db/db) mice show metabolic responsiveness to insulin. *Am. J. Physiol. Heart Circ. Physiol.* **290**, H1763-1769 (2006).
15. Egom, E. E. *et al.* Impaired sinoatrial node function and increased susceptibility to atrial fibrillation in mice lacking natriuretic peptide receptor C. *J. Physiol.* **593**, 1127–1146 (2015).
16. Mackasey, M. *et al.* Natriuretic peptide receptor-C protects against angiotensin II-mediated sinoatrial node disease in mice. *JACC Basic Transl. Sci.* **3**, 824–843 (2018).
17. Moghtadaei, M. *et al.* The impacts of age and frailty on heart rate and sinoatrial node function. *J. Physiol.* **594**, 7105–7126 (2016).
18. Clark, R. B. *et al.* A rapidly activating delayed rectifier K+ current regulates pacemaker activity in adult mouse sinoatrial node cells. *Am. J. Physiol. Heart Circ. Physiol.* **286**, H1757-1766 (2004).
19. Cifelli, C. *et al.* RGS4 regulates parasympathetic signaling and heart rate control in the sinoatrial node. *Circ. Res.* **103**, 527–535 (2008).
20. Ishii, M., Inanobe, A. & Kurachi, Y. PIP3 inhibition of RGS protein and its reversal by Ca^{2+}/calmodulin mediate voltage-dependent control of the G protein cycle in a cardiac K^+ channel. *Proc. Natl. Acad. Sci. U. S. A.* **99**, 4325–4330 (2002).
21. Oudit, G. Y. *et al.* The role of phosphoinositide-3 kinase and PTEN in cardiovascular physiology and disease. *J. Mol. Cell. Cardiol.* **37**, 449–471 (2004).
22. Bertrand, L., Horman, S., Beauloye, C. & Vanoverschelde, J. L. Insulin signalling in the heart. *Cardiovasc. Res.* **79**, 238–248 (2008).
23. Wickman, K., Nemec, J., Gendler, S. J. & Clapham, D. E. Abnormal heart rate regulation in GIRK4 knockout mice. *Neuron* **20**, 103–114 (1998).
24. Mesirca, P. *et al.* The G-protein-gated K+ channel, IKACh, is required for regulation of pacemaker activity and recovery of resting heart rate after sympathetic stimulation. *J. Gen. Physiol.* **142**, 113–126 (2013).
25. Lomax, A. E., Rose, R. A. & Giles, W. R. Electrophysiological evidence for a gradient of G protein-gated K+ current in adult mouse atria. *Br. J. Pharmacol.* **140**, 576–584 (2003).
26. Bender, K. *et al.* Acute desensitization of GIRK current in rat atrial myocytes is related to K+ current flow. *J. Physiol.* **561**, 471–483 (2004).
27. Shui, Z., Boyett, M. R., Zang, W. J., Haga, T. & Kameyama, K. Receptor kinase-dependent desensitization of the muscarinic K+ current in rat atrial cells. *J. Physiol.* **487**(Pt 2), 359–366 (1995).
28. Doupnik, C. A., Davidson, N., Lester, H. A. & Kofuji, P. RGS proteins reconstitute the rapid gating kinetics of gbetagamma-activated inwardly rectifying K+ channels. *Proc. Natl. Acad. Sci. U. S. A.* **94**, 10461–10466 (1997).
29. Roman, D. L., Blazer, L. L., Monroy, C. A. & Neubig, R. R. Allosteric inhibition of the regulator of G protein signaling-Galpha protein–protein interaction by CCG-4986. *Mol. Pharmacol.* **78**, 360–365 (2010).
30. Roman, D. L. *et al.* Identification of small-molecule inhibitors of RGS4 using a high-throughput flow cytometry protein interaction assay. *Mol. Pharmacol.* **71**, 169–175 (2007).
31. Fu, Y., Huang, X., Piao, L., Lopatin, A. N. & Neubig, R. R. Endogenous RGS proteins modulate SA and AV nodal functions in isolated heart: Implications for sick sinus syndrome and AV block. *Am. J. Physiol. Heart Circ. Physiol.* **292**, H2532-2539 (2007).
32. Fu, Y. *et al.* Endogenous RGS proteins and Galpha subtypes differentially control muscarinic and adenosine-mediated chronotropic effects. *Circ. Res.* **98**, 659–666 (2006).
33. Yang, J. *et al.* RGS6, a modulator of parasympathetic activation in heart. *Circ. Res.* **107**, 1345–1349 (2010).
34. Ishii, M., Fujita, S., Yamada, M., Hosaka, Y. & Kurachi, Y. Phosphatidylinositol 3,4,5-trisphosphate and Ca^{2+}/calmodulin competitively bind to the regulators of G-protein-signalling (RGS) domain of RGS4 and reciprocally regulate its action. *Biochem. J.* **385**, 65–73 (2005).
35. Popov, S. G., Krishna, U. M., Falck, J. R. & Wilkie, T. M. Ca^{2+}/Calmodulin reverses phosphatidylinositol 3,4, 5-trisphosphate-dependent inhibition of regulators of G protein-signaling GTPase-activating protein activity. *J. Biol. Chem.* **275**, 18962–18968 (2000).
36. Abel, E. D. Insulin signaling in heart muscle: Lessons from genetically engineered mouse models. *Curr. Hypertens. Rep.* **6**, 416–423 (2004).
37. Posokhova, E., Wydeven, N., Allen, K. L., Wickman, K. & Martemyanov, K. A. RGS6/Gss5 complex accelerates IKACh gating kinetics in atrial myocytes and modulates parasympathetic regulation of heart rate. *Circ. Res.* **107**, 1350–1354 (2010).
38. Zhang, Y. *et al.* Electrical conduction system remodeling in streptozotocin-induced diabetes mellitus rat heart. *Front. Physiol.* **10**, 826 (2019).
39. Luo, M. *et al.* Diabetes increases mortality after myocardial infarction by oxidizing CaMKII. *J. Clin. Investig.* **123**, 1262–1274 (2013).
40. Soltysinska, E., Speerschneider, T., Winther, S. V. & Thomsen, M. B. Sinoatrial node dysfunction induces cardiac arrhythmias in diabetic mice. *Cardiovasc. Diabetol.* **13**, 122 (2014).
41. Howarth, F. C. *et al.* The pattern of mRNA expression is changed in sinoatrial node from Goto-Kakizaki Type 2 diabetic rat heart. *J. Diabetes. Res.* **2018**, 8454078 (2018).
42. Polina, I. *et al.* Loss of insulin signaling may contribute to atrial fibrillation and atrial electrical remodeling in type 1 diabetes. *Proc. Natl. Acad. Sci. U. S. A.* **117**, 7990–8000 (2020).

Acknowledgements

We acknowledge Megan McRae, Erin Seto, Adam Kirkby, and Sara Rafferty for technical support and experimental assistance. This work was supported by the Canadian Institutes of Health Research to R.A.R. (MOP 142486 and PJT 166105). Y.L. holds a Canadian Institutes of Health Research Fellowship. H.J.J. was supported by a Killam Postdoctoral Fellowship and a Libin Cardiovascular Institute Postdoctoral Fellowship.

Author contributions

The conception of the experiments was by Y.L. and R.A.R. The design of the experiments was by Y.L., H.J.J., P.S.K., O.B. and R.A.R. The collection, analysis and interpretation of the data was by Y.L., H.J.J., P.S.K., O.B. and R.A.R. Drafting the article or revising it critically for important intellectual content was done by Y.L., H.J.J. and R.A.R. All authors approved the final version of the manuscript.

Competing interests

The authors declare no competing interests.

Additional information

Supplementary Information The online version contains supplementary material available at https://doi.org/10.1038/s41598-021-91937-2.

Correspondence and requests for materials should be addressed to R.A.R.

Supplemental Material

Impaired regulation of heart rate and sinoatrial node function by the parasympathetic nervous system in type 2 diabetic mice

Yingjie Liu[a], Hailey J. Jansen[a], Pooja S. Krishnaswamy[b], Oleg Bogachev[b], Robert A. Rose[a*]

[a]Libin Cardiovascular Institute
Department of Cardiac Sciences
Department of Physiology and Pharmacology
Cumming School of Medicine
University of Calgary
Calgary, Alberta, Canada

[b]Department of Physiology and Biophysics
Dalhousie University
Halifax, Nova Scotia, Canada

Supplemental Methods

Animals

Male and female littermate wildtype and db/db mice[1] between the ages of 16 and 20 weeks were used in this study. This mouse contains an autosomal recessive mutation in the leptin receptor (*Lepr*) gene. Mice homozygous for the mutation display hyperphagia and hyperglycemia[2]. Db/db mice were initially obtained from the Jackson Laboratory (strain C57BL/6J-*Lepr*^{db}) and then bred locally. Homozygous db/db mice and wildtype littermates were used in this study. Animals were fed *ad libitum* and kept on a 12:12 h light-dark cycle. At the age range used in this study db/db mice were overtly obese and hyperglycemic as we have shown previously[3].

Intracardiac electrophysiology and electrocardiogram recording

Surface ECGs (used to assess changes in heart rate) were measured in anesthetized mice (2% isoflurane inhalation) using 30 gauge subdermal needle electrodes (Grass Technologies). A 1.2 french octapolar electrophysiology catheter containing 8 electrodes spaced 0.5 mm apart (Transonic) was used for intracardiac pacing experiments. Correct catheter placement was ensured by obtaining a ventricular signal in the distal lead and a predominant atrial signal in the proximal lead. Sinoatrial node recovery time (SNRT) was measured by delivering a 12 stimulus drive train at a cycle length of 100 ms. SNRT is defined as the time between the last stimulus in the drive train and the occurrence of the first spontaneous atrial beat (P wave). SNRT was corrected for heart rate (cSNRT) by subtracting the prestimulus RR interval from the measured SNRT. All ECG data were acquired using a Gould ACQ-7700 amplifier and Ponemah Physiology Platform software (Data Sciences International) as we have described previously[4,5]. Body temperature was maintained at 37˚C using a heating pad. CCh and atropine were delivered by intraperitoneal injection.

Isolation of mouse sinoatrial node myocytes

Mouse SAN myocytes were isolated using procedures we have described previously[6-8]. Mice were administered a 0.2 ml intraperitoneal injection of heparin (1000 IU/ml) to prevent blood clotting. Following this, mice were anesthetized by isoflurane inhalation and then sacrificed by cervical dislocation. The heart was excised into Tyrode's solution (35ºC) consisting of (in mM) 140 NaCl, 5.4 KCl, 1.2 KH_2PO_4, 1.0 $MgCl_2$, 1.8 $CaCl_2$, 5.55 glucose, and 5 HEPES, with pH adjusted to 7.4 with NaOH. Atrial preparations were dissected and the SAN region was cut into strips, which were transferred and rinsed in a 'low Ca^{2+}, Mg^{2+} free' solution containing (in mM) 140 NaCl, 5.4 KCl, 1.2 KH_2PO_4, 0.2 $CaCl_2$, 50 taurine, 18.5 glucose, 5 HEPES and 1 mg/ml bovine serum albumin (BSA), with pH adjusted to 6.9 with NaOH. SAN tissue strips were digested in 5 ml of 'low Ca^{2+}, Mg^{2+} free' solution containing collagenase (type II, Worthington Biochemical Corporation), elastase (Worthington Biochemical Corporation) and protease (type XIV, Sigma Chemical Company) for 30 min. The tissue was then transferred to 5 ml of modified KB solution containing (in mM) 100 potassium glutamate, 10 potassium aspartate, 25 KCl, 10 KH_2PO_4, 2 $MgSO_4$, 20 taurine, 5 creatine, 0.5 EGTA, 20 glucose, 5 HEPES, and 0.1% BSA, with pH adjusted to 7.2 with KOH. The tissue was mechanically agitated using a wide-bore pipette. This procedure yielded individual SAN myocytes with cellular automaticity that was recovered after readapting the cells to a physiological concentration of Ca^{2+}. SAN myocytes were identified by their small spindle shape and ability to beat spontaneously in the recording chamber when superfused with normal Tyrode's solution. When patch-clamped, SAN myocytes always displayed spontaneous action potentials. The capacitance of single SAN myocytes was 20 – 35 pF.

Solutions and electrophysiological protocols

Spontaneous action potentials, as well as the acetylcholine activated K^+ current (I_{KACh}), the hyperpolarization activated current (I_f) and the rapid delayed rectifier K^+ current (I_{Kr}) were recorded in single SAN myocytes using the patch-clamp technique in the whole cell configuration[9,10]. Action potentials and ionic currents were recorded at room temperature (22-23°C). I_{KACh} was investigated using a voltage ramp from +50 mV to -120 mV (holding potential was -80 mV) before and after application of carbachol (CCh; 10 µM) as we have described previously[10]. I_{KACh} was quantified as the CCh-sensitive difference current. I_f was recorded by applying a series of 2.5 s voltage clamp steps between -150 mV and -30 mV, followed by a step to -130 mV, from a holding potential of -35 mV. Activation kinetics for I_f were determined by normalizing tail currents at each voltage to the maximum current level at -130 mV and fitting the data to the Boltzmann function: $I/I_{max}=1/(1+\exp[(V_m-V_{1/2})/k])$ where V_m is the potential of the voltage clamp step, $V_{1/2}$ is the voltage at which 50% activation occurs and k is the slope factor. I_{Kr} was recorded by applying a series of 1 s voltage clamp steps between -50 and +50 mV, followed by a 2 s step to -45 mV to elicit I_{Kr} tail currents[11]. I_{Kr} tail currents were fit to the Boltzmann function: $I=I_{max}/(1+\exp(V_m-V_{1/2})/k)$ where V_m is the potential of the voltage clamp step, $V_{1/2}$ is the voltage at which 50% activation occurs and k is the slope factor[11].

For recording APs, I_{KACh}, I_{Kr} and I_f, the recording chamber was superfused with a normal Tyrode's solution (22 – 23ºC) containing (in mM) 140 NaCl, 5 KCl, 1 $MgCl_2$, 1 $CaCl_2$, 10 HEPES, and 5 glucose, with pH adjusted to 7.4 with NaOH. The pipette filling solution for APs, I_{KACh}, I_{Kr} and I_f, contained (in mM) 135 KCl, 0.1 $CaCl_2$, 1 $MgCl_2$, 5 NaCl, 10 EGTA, 4 Mg-ATP, 6.6 Na-phosphocreatine, 0.3 Na-GTP and 10 HEPES, with pH adjusted to 7.2 with KOH. 2 mM $BaCl_2$ was added to the superfusate when recording I_f in order to block I_{KACh}[12].

Micropipettes were pulled from borosilicate glass (with filament, 1.5 mm OD, 0.75 mm ID, Sutter Instrument Company) using a Flaming/Brown pipette puller (model p-87, Sutter Instrument Company). The resistance of these pipettes was 4 – 8 MΩ when filled with recording solution. Micropipettes were positioned with a micromanipulator (Burleigh PCS-5000 system)

mounted on the stage of an inverted microscope (Olympus IX71). Seal resistance was 2 – 15 GΩ. Rupturing the sarcolemma in the patch experiments resulted in access resistances of 5 – 15 MΩ. Series resistance compensation averaged 80 – 85% using an Axopatch 200B amplifier (Molecular Devices). Data were digitized using a Digidata 1440 and pCLAMP 10 software (Molecular Devices) and stored on computer for analysis.

Spontaneous AP parameters, including the maximum diastolic potential (MDP), the slope of the diastolic depolarization (DD slope) and the take-off potential were analyzed as described previously[13-15]. The DD slope was measured by fitting a straight line to the initial linear portion (~2/3) of this AP component as we and other have previously done[6,7,14,16].

Quantitative PCR

Quantitative gene expression was measured in the SAN as we have described previously[4,6,17]. Intron-spanning primers were designed for *Chrm2* (M_2R), *Kcnj3* ($K_{ir}3.1$), *Kcnj5* ($K_{ir}3.4$), *Hcn1*, *Hcn2*, and *Hcn4*. Glyceraldehyde 3-phosphate dehydrogenase (GAPDH) was used as a reference gene. Primer sequences are listed in Supplemental Table 2 below.

Total RNA was isolated from the SAN using a PureZOL™ RNA Isolation Reagent and the Aurum™ Total RNA Fatty and Fibrous Tissue Kit (Bio-Rad Laboratories) as per kit instructions. RNA samples were eluted from the spin column in 40 µL elution buffer. RNA yield and purity were assessed using a Nanodrop. All samples had a A_{260}/A_{280} of over 2.0 and therefore were free of DNA contamination. Next, cDNA (2.5 ng/µL) was synthesized using the iScript™ cDNA Synthesis Kit (Bio-Rad Laboratories). Reactions were performed in a Bio-Rad MyCycler thermal cycler using the following protocol: 5 min of priming at 25ºC followed by reverse transcription for 30 min at 42ºC then 5 min at 85ºC to inactivate reverse transcriptase.

All qPCR reactions were run in duplicate in 10 µL reactions that contained the following: 4 µL sample cDNA, 5.6 µL GoTaq® qPCR Master Mix (Promega), and 0.4 µL primers. Primers were reconstituted to a final concentration of 100 µM with nuclease free water and stored at -

20ºC until use. Primers were diluted to 10 µM for qPCR reactions. RT-qPCR reactions were performed using the CFX96 Touch™ Real-Time PCR Detection System (Bio-Rad) using the following protocol: Taq polymerase was activated for 2 min at 95ºC followed by 39 cycles of denaturing for 15 s at 95ºC, annealing for 30 s at 60ºC, and extension for 30s at 72ºC. This was followed by melt curve analysis from 65-95ºC in 0.5ºC increments. Data were analyzed using the $2^{-\Delta\Delta C_T}$ method using the CFX Manager Software version 3.1 (Bio-Rad). Gene expression was normalized to GAPDH.

Western blotting

Protein samples were extracted from two SANs and pooled for each experimental replicate in order to ensure sufficient protein, as we[6] and others[18] have described previously. Tissues were pre-cooled in liquid nitrogen and homogenized in an ice-cold RIPA buffer (50mM Tris, 150mM NaCl, 1mM EDTA, 25mM sucrose, 1% Triton, 0.1% SDS) containing 0.5mM DTT (1,4-Dithiothreitol, Roche) and Protease Inhibitor Cocktail (Sigma-Aldrich). Preparation was centrifuged at 10000 rpm at 4^0C for 10 min and supernatant was collected. Protein concentrations were measured using a Bio-Rad DC Protein Assay Kit II (Bio-Rad). Protein samples (20 µg/lane) were prepared in Laemmli sample buffer (Bio-Rad) containing 355 mM 2-marcaptoethanol (Bio-Rad) separated by 7.5% SDS-polyacrylamide gels (SDS-PAGE) and transferred onto Biotrace™ NT nitrocellulose Transfer Membrane (VWR). The membrane was blocked with 1% casein in tris-buffered saline (TBS; Bio-Rad) for 1 hour and incubated overnight at 4^0C with rabbit primary antibodies separately including HCN1 1:500 (Alomone Labs), HCN2 1:500 (Alomone Labs), HCN4 1:500 (Alomone Labs), M_2R 1:500 (Abcam), $K_{ir}3.1$ 1:1000 (Abcam), $K_{ir}3.4$ 1:1000 (Abcam) and RGS4 1:500 (Aviva Systems Biology). The membrane was washed 3 times with TBST (TBS with 1% Tween 20 (Bio-Rad)) and incubated with StarBright700 anti-Rabbit secondary antibody (Bio-Rad) at 1:10000 together with Rhodamine anti-GAPDH at 1:5000 (Bio-Rad) for 1 hour at room temperature. Then the membrane was

washed again 3 times with TBST and scanned using the ChemiDoc system (Bio-Rad). We quantified expression of each of these proteins based on the identification of bands at the predicted molecular weight according to the information from the supplier.

Supplemental Figures

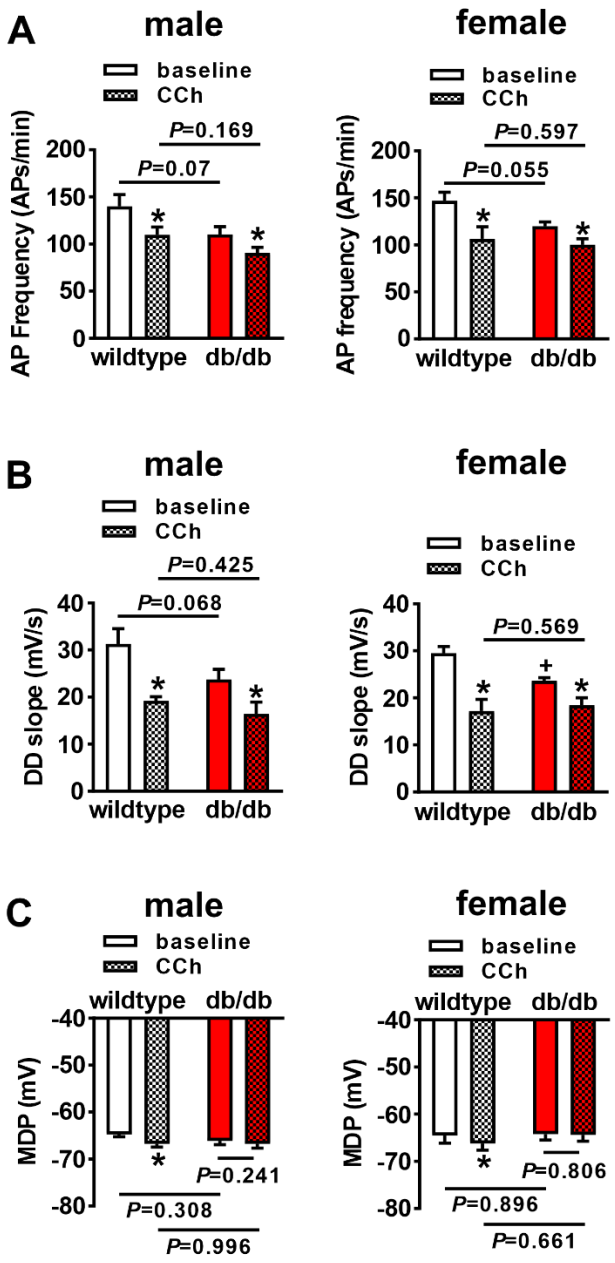

Figure S1: Comparison of spontaneous action potential parameters in isolated sinoatrial node myocytes from male and female db/db mice. A: Summary of spontaneous AP frequency at baseline and after CCh (50 nM) in male and female SAN myocytes from wildtype and db/db mice. **B:** Summary of DD slope at baseline and after CCh (50 nM) in male and female SAN myocytes from wildtype and db/db mice. **C:** Summary of MDP at baseline and after CCh (50 nM) in male and female SAN myocytes from wildtype and db/db mice. For all panels *n*=10 wildtype male cells, 7 db/db male cells, 4 wildtype female cells and 6 db/db female cells. **P*<0.05 vs. baseline; $^{+}$*P*<0.05 vs wildtype by two way repeated measures ANOVA with Holm-Sidak posthoc test.

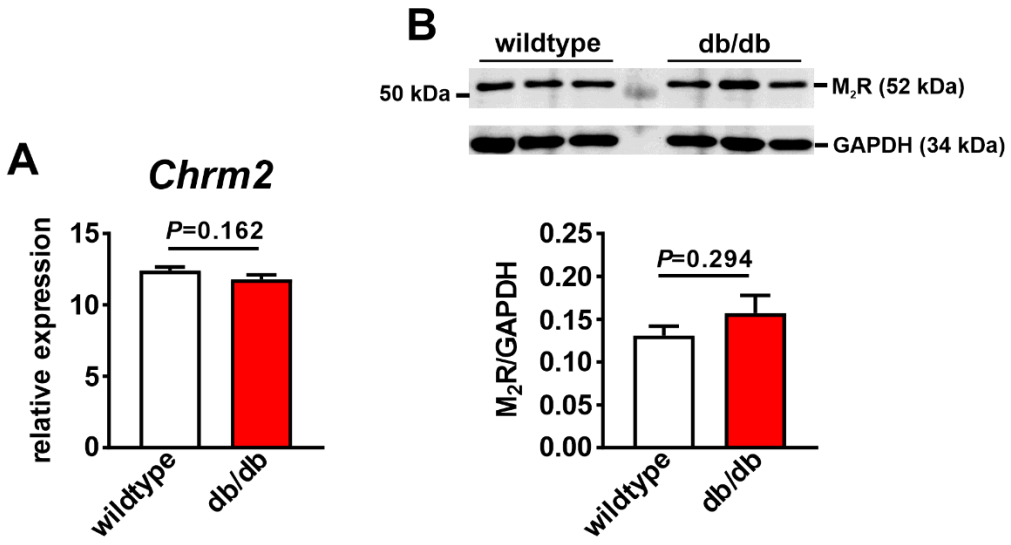

Figure S2: Muscarinic (M_2) receptor gene and protein expression in the SAN in db/db mice. **A:** mRNA expression of *Chrm2* in wildtype (*n*=8) and db/db (*n*=8) SAN. Data analyzed by Student's *t*-test. **B:** Representative Western blot and summary protein expression for M_2 receptor (M_2R) in wildtype (*n*=6) and db/db (*n*=6) SAN. Data analyzed by Student's *t*-test. Uncropped Western blot provided Supplemental Fig. S6.

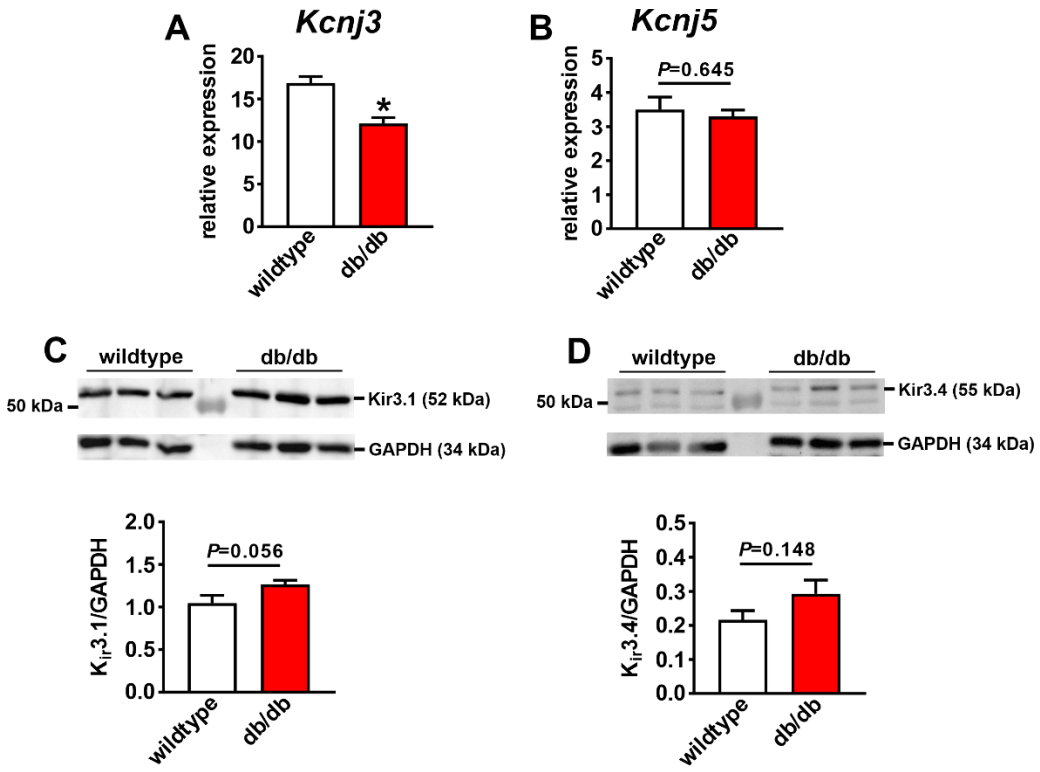

Figure S3: Gene and protein expression of I_{KACh} subunits in the SAN in db/db mice. **A and B:** mRNA expression of *Kcnj3* (**A**) and *Kcnj5* (**B**) in wildtype (n=8) and db/db (n=8) SAN. *P<0.05 vs wildtype by Student's t-test. **C and D:** Representative Western blots and summary protein expression for $K_{ir}3.1$ (**C**) and $K_{ir}3.4$ (**D**) in wildtype (n=6) and db/db (n=6) SAN. Data analyzed by Student's t-test. Uncropped Western blots provided Supplemental Fig. S6.

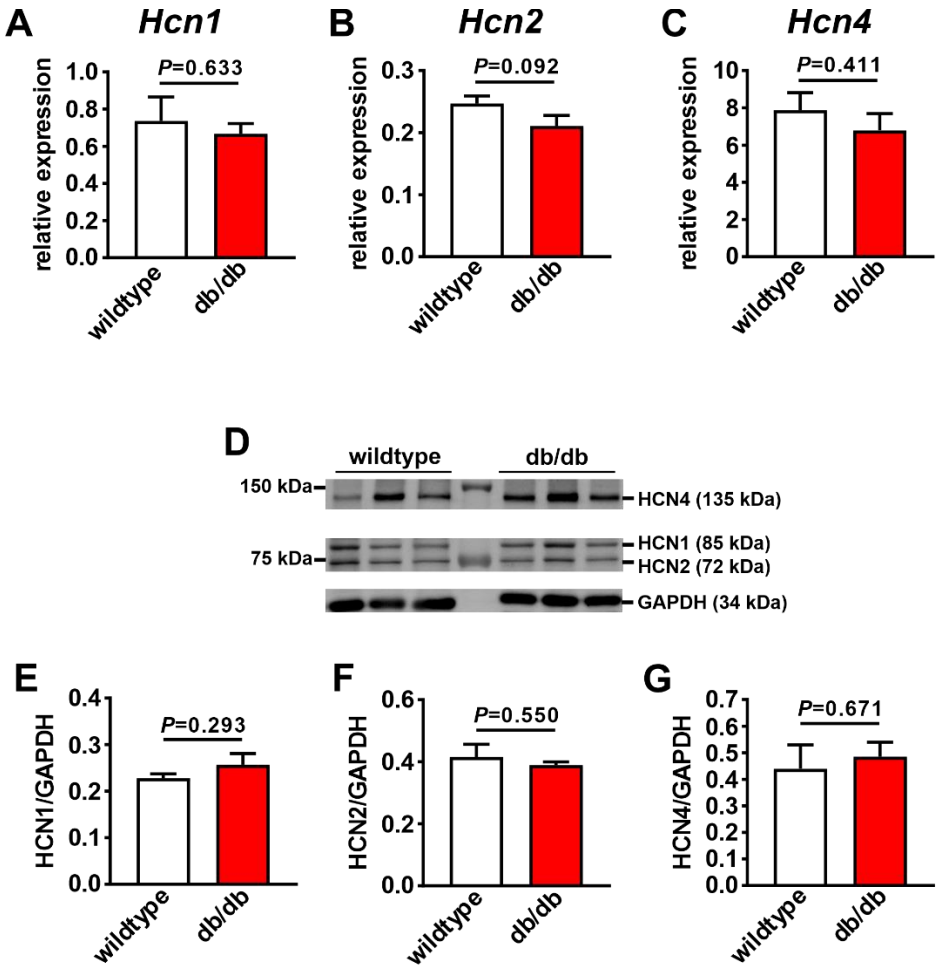

Figure S4: Gene and protein expression of I_f subunits in the SAN in db/db mice. **A-C:** mRNA expression of *Hcn1* (**A**), *Hcn2* (**B**) and *Hcn4* (**C**) in wildtype (n=16) and db/db (n=14) SAN. Data analyzed by Student's t-test. **D:** Representative Western blot for HCN1, HCN2 and HCN4. **E-G:** Summary protein expression for HCN1 (**E**), HCN2 (**F**) and HCN4 (**G**) in wildtype (n=6) and db/db (n=6) SAN. Data analyzed by Student's t-test. Uncropped Western blot provided Supplemental Fig. S6.

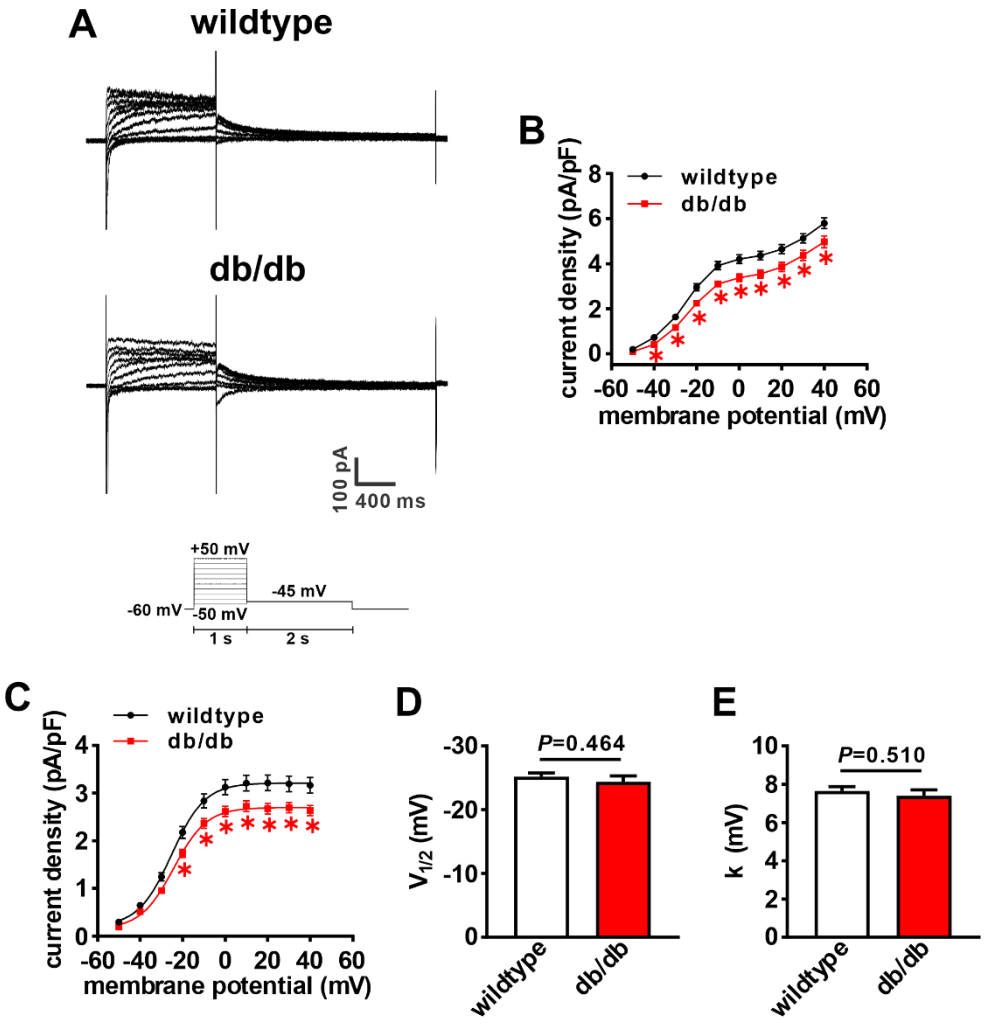

Figure S5: Rapidly activated delayed rectifier K^+ current (I_{Kr}) in db/db SAN myocytes. **A:** Representative I_K recordings in wildtype and db/db SAN myocytes. Voltage protocol shown at bottom of recordings. **B:** I_K IV relationship at the end of the 1 s voltage clamp step in wildtype (n=53) and db/db (n=42) SAN myocytes. *P<0.05 vs wildtype by two-way repeated measures ANOVA with Holm-Sidak posthoc test. **C:** Boltzmann fit of I_{Kr} tail current in wildtype and db/db SAN myocytes. *P<0.05 vs wildtype by two-way ANOVA with Holm-Sidak posthoc test. **D:** Voltage for 50% channel activation ($V_{1/2(act)}$) for I_{Kr} tail current in wildtype and db/db SAN myocytes. **E:** slope factor (k) for I_{Kr} tail currents in wildtype and db/db SAN myocytes. For panels **D** and **E** data analyzed by Student's t-test.

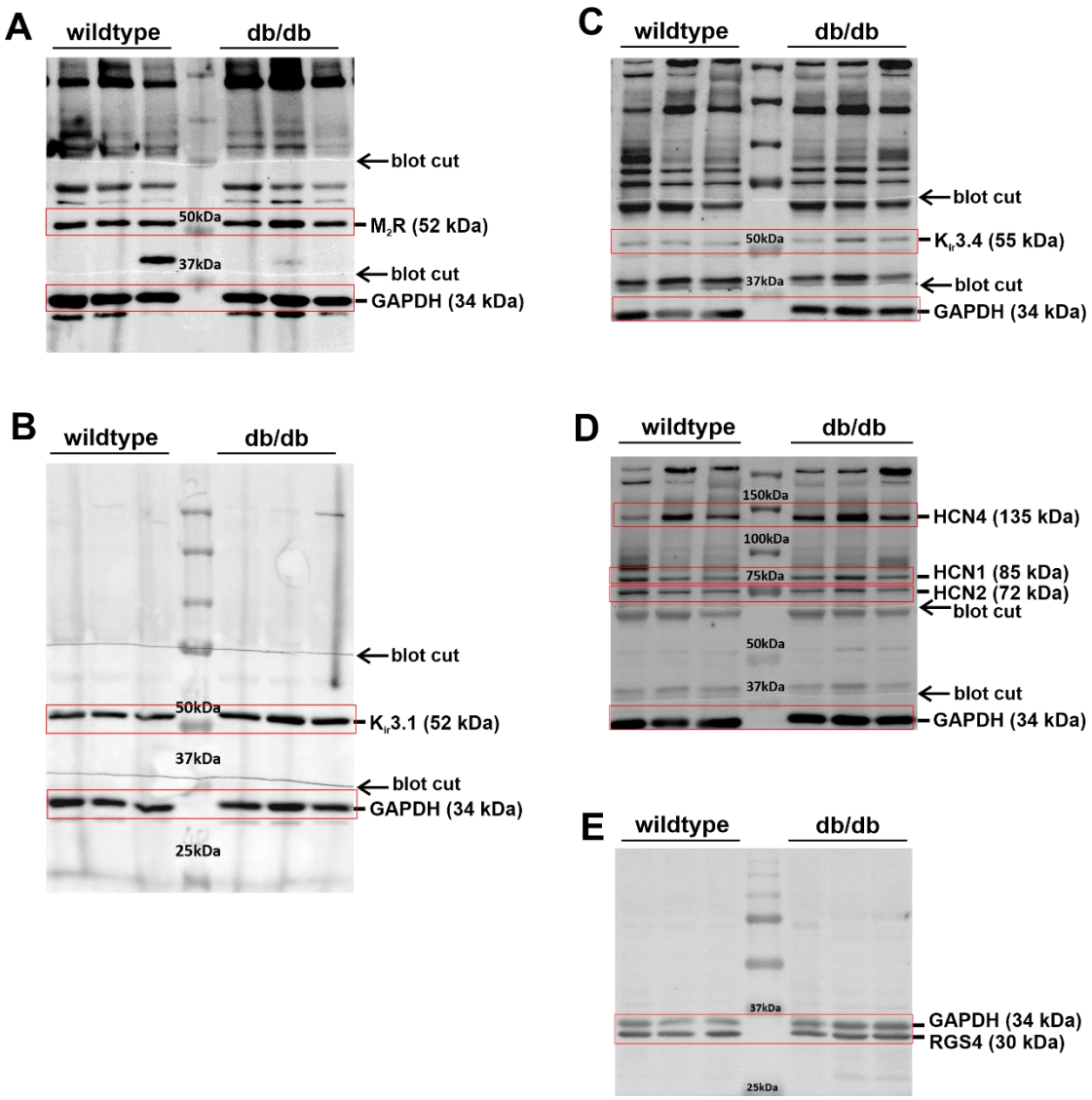

Figure S6: Uncropped Western blots. Full, uncropped representative Western blots for M_2R (**A**), $K_{ir}3.1$ (**B**), $K_{ir}3.4$ (**C**), HCN channels (**D**) and RGS4 (**E**) in the SAN in wildtype and db/db mice. HCN channels and $K_{ir}3.4$ were run on the same blot (panels C and D, which are presented at different contrasts). Red boxes indicate regions that were cropped and presented in figures within the manuscript. Note that membranes in panels A, B C and D were cut, as indicated by arrows, so that multiple proteins could be assessed on the same blot.

Supplemental Table 1: I_f activation kinetics in db/db mice

	wildtype		**db/db**	
	baseline	**CCh**	**baseline**	**CCh**
$V_{1/2(act)}$ (mV)	-107.9±0.4	-111.4±0.4*	-108.1±0.4	-112.3±.04*
k (mV)	13.4±0.4	13.0±0.4	14.3±0.3	14.3±0.4

$V_{1/2(act)}$, voltage for 50% channel activation; k, slope factor. *P<0.05 vs baseline by two-way repeated measures ANOVA with Holm-Sidak posthoc test; n=15 SAN myocytes for wildtype and 16 SAN myocytes for db/db.

Supplemental Table 2: Quantitative PCR primers

Gene of Interest	**Forward Primer (5' → 3')**	**Reverse Primer (5' → 3')**	**Amplicon Length**
Chrm2	AGTGTGGACAATTGGCTACTGG	ACCTTGTAGCGCCTATGTTCT	140
Kcnj3	AAACTCACTCTCATGTTCCG	TCCAGTTCAAGTTGGTCAAG	134
Kcnj5	AGATAGAAGGGCGAGGCAGA	CCCTTGGGGCTAACTTCTGG	192
HCN1	CTCTTTTTGCTAACGCCGAT	CATTGAAATTGTCCACCGAA	291
HCN2	CTTCACCAAGATCCTCAGTCTG	GGTCGTAGGTCATGTGGAAA	92
HCN4	CCAGGAGAAGTATAAACAGGTGGAGCG	GTTGATGATCTCCTCTCGAAGTGGCTC	169
gapdh	AATGGGGTGAGGCCGGTGCT	CACCCTTCAAGTGGGCCCCG	87

1. Hsueh, W. *et al.* Recipes for creating animal models of diabetic cardiovascular disease. *Circ. Res.* **100**, 1415-1427 (2007).
2. Coleman, D. L. Obese and diabetes: two mutant genes causing diabetes-obesity syndromes in mice. *Diabetologia* **14**, 141-148 (1978).
3. Bohne, L. J. *et al.* Electrical and structural remodeling contribute to atrial fibrillation in type 2 diabetic db/db mice. *Heart Rhythm* **18**, 118-129 (2021).
4. Egom, E. E. *et al.* Impaired sinoatrial node function and increased susceptibility to atrial fibrillation in mice lacking natriuretic peptide receptor C. *J. Physiol.* **593**, 1127-1146 (2015).
5. Jansen, H. J. *et al.* Atrial structure, function and arrhythmogenesis in aged and frail mice. *Sci. Rep.* **7**, 44336 (2017).
6. Mackasey, M. *et al.* Natriuretic Peptide Receptor-C Protects Against Angiotensin II-Mediated Sinoatrial Node Disease in Mice. *JACC Basic Transl. Sci.* **3**, 824-843 (2018).
7. Krishnaswamy, P. S. *et al.* Altered parasympathetic nervous system regulation of the sinoatrial node in Akita diabetic mice. *J. Mol. Cell. Cardiol.* **82**, 125-135 (2015).
8. Rose, R. A., Lomax, A. E., Kondo, C. S., Anand-Srivastava, M. B. & Giles, W. R. Effects of C-type natriuretic peptide on ionic currents in mouse sinoatrial node: a role for the NPR-C receptor. *Am. J. Physiol. Heart Circ Physiol* **286**, H1970-1977 (2004).
9. Hamill, O. P., Marty, A., Neher, E., Sakmann, B. & Sigworth, F. J. Improved patch-clamp techniques for high-resolution current recording from cells and cell-free membrane patches. *Pflugers Arch.* **391**, 85-100 (1981).
10. Lomax, A. E., Rose, R. A. & Giles, W. R. Electrophysiological evidence for a gradient of G protein-gated K+ current in adult mouse atria. *Br. J. Pharmacol.* **140**, 576-584 (2003).
11. Clark, R. B. *et al.* A rapidly activating delayed rectifier K+ current regulates pacemaker activity in adult mouse sinoatrial node cells. *Am. J. Physiol. Heart Circ Physiol* **286**, H1757-1766 (2004).
12. DiFrancesco, D. & Tromba, C. Inhibition of the hyperpolarization-activated current (if) induced by acetylcholine in rabbit sino-atrial node myocytes. *J. Physiol.* **405**, 477-491 (1988).
13. Mangoni, M. E. & Nargeot, J. Properties of the hyperpolarization-activated current (I(f)) in isolated mouse sino-atrial cells. *Cardiovasc. Res.* **52**, 51-64 (2001).
14. Springer, J. *et al.* The natriuretic peptides BNP and CNP increase heart rate and electrical conduction by stimulating ionic currents in the sinoatrial node and atrial myocardium following activation of guanylyl cyclase-linked natriuretic peptide receptors. *J. Mol. Cell. Cardiol.* **52**, 1122-1134 (2012).
15. Azer, J., Hua, R., Vella, K. & Rose, R. A. Natriuretic peptides regulate heart rate and sinoatrial node function by activating multiple natriuretic peptide receptors. *J. Mol. Cell. Cardiol.* **53**, 715-724 (2012).
16. Honjo, H., Boyett, M. R., Kodama, I. & Toyama, J. Correlation between electrical activity and the size of rabbit sino-atrial node cells. *J. Physiol.* **496 (Pt 3)**, 795-808 (1996).
17. Moghtadaei, M. *et al.* The impacts of age and frailty on heart rate and sinoatrial node function. *J. Physiol.* **594**, 7105-7126 (2016).
18. El Khoury, N. *et al.* Upregulation of the hyperpolarization-activated current increases pacemaker activity of the sinoatrial node and heart rate during pregnancy in mice. *Circulation* **127**, 2009-2020 (2013).